BL35XU
Inelastic and Nuclear Resonant Scattering

1. Introduction

Since 2021A, BL35XU has been operated for research using two techniques: inelastic X-ray scattering (IXS) and nuclear resonant scattering (NRS). These techniques are both flux-limited and strongly benefit from the short (20 mm)-period insertion device at BL35XU. Both techniques also use a high-, meV-, energy resolution or better. In FY2024, several tests and developments were conducted to improve performance and expand research interests, as described below.

2. Nonresonant high-energy-resolution inelastic X-ray scattering

The IXS station at BL35XU uses high-resolution IXS to investigate atomic motion–phonon dispersion in crystals and excitations in liquids. This station has a 3×4 analyzer array that enables the measurement of IXS spectra at 12 Q positions at one arm position. IXS is particularly notable as it allows access to small (micron-scale) samples, including thin films, which is not possible with other methods (e.g., inelastic neutron scattering). Although the IXS energy resolution is typically 1.5 or 3 meV, recent operation has been carried out only with the 1.5 meV setup.

We have launched a series of activities this year aimed at improving energy resolution, based on studies at BL43LXU [1,2]. While the pixel detector, an essential instrument of this improvement, is temporarily borrowed from RIKEN MDG, we have developed a detector mounting device, image processing software for IXS measurements, and an analyzer mount designed to apply a temperature gradient to the analyzer.

The new detector should be positioned at the same distance from the analyzer array as the previous 12-single-element detector. Unlike the old detector, which operated in vacuum, the new one functions in air, requiring a redesigned mounting device.

This update also prompted a review of the post-sample slit installation. A four-blade slit is typically used to suppress stray light, while a Soller slit unit is employed in special cases (e.g., thin-film samples). However, the permanent installation of the Soller slit is difficult because it requires a swivel

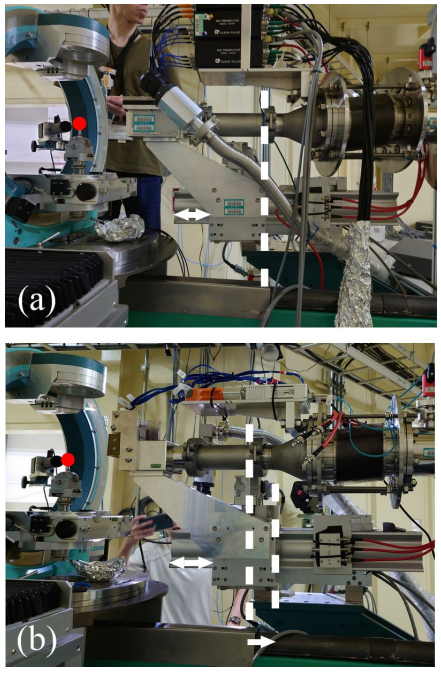

Fig. 1. Old (a) and new (b) detectors, and mounting devices. The mounting position has been shifted by about 40 mm, as shown by arrows. The sample position is indicated by the red sphere.

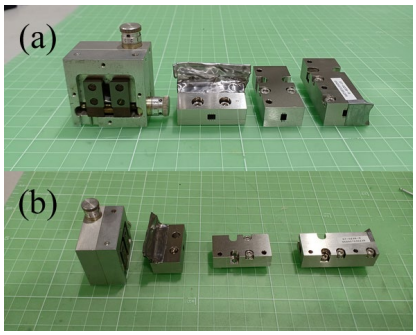

Fig. 2. Soller slit units (three on the right) and the four-blade slit (left). (a) Front view. (b) Side view.

stage and two translational stages for precise positioning, which risks mechanical interference with a stage mounting an instrument (the hth stage). To address this, we have rearranged the detector height stage and the Soller slit stages, and replaced their holding arms (Fig. 1). We also fabricated two new Soller slit units, one of which is dimensionally compatible with the four-blade slit (Fig. 2). As a result, previously used sample-environment devices can be mounted on the hth stage without any issues.

The new detector is a CdTe-pixel detector (LAMBDA FLEX CdTe) with a pixel size of 55 μm. Since the single-element size of the previous detector is 2 mm square, the region of interest (ROI) was set to 40 × 40 pixels to achieve the same detection area. This means that areas previously treated as a single data point can now be spatially resolved into finer data points. This position-resolved data enables dispersion compensation [3], which further corrects for the angular dependence of energy within the ROI. As a result, the energy spread at each data point is reduced, contributing to an improved energy resolution. The energy resolution is also affected by the scattering angle that corresponds to the ROI position for each analyzer. While it is possible to configure an ROI for a particular analyzer to minimize the energy resolution, we strategically adjusted the analyzer angles and the ROI arrangement to achieve a uniform and acceptable energy resolution across all analyzers.

We also upgraded the data acquisition and processing software to fully utilize the new 2D detector. In IXS experiments, which typically have relatively low count rates, the detector captures many sparse images. Instead of storing full images, we extract only the essential pixel data and save it in a compact text format [4], preserving essential information while reducing data size. In data processing, we introduced new fitting parameters (mpl: meV per line) to account for energy deviation between each row in the ROI and optimized them using resolution function data. These upgrades improved the energy resolution with the best-aligned analyzer from 1.46 to 1.35 meV. The optimized mpl was −0.030 meV, which means that the energy deviation between each line in the ROI is 0.030 meV (the sign represents the direction of energy dispersion).

The last component for improving energy resolution is the analyzer holder, which applies a temperature gradient. This year, we made a test unit

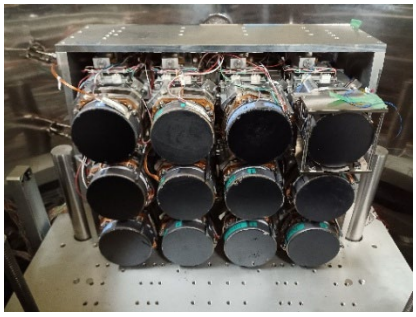

Fig. 3. Resent analyzer array at BL35XU. The one at the top right is with the temperature-gradient holder.

for one of the 12 analyzers (Fig. 3). The key challenges included fitting the holder within a limited space without altering the sample distance and applying a gradient to a circular analyzer (not rectangular as those in BL43LXU). The design minimizes contact points to the analyzer, creating space for heaters. Figure 4 shows temperature changes at three locations expected to be the hottest, intermediate, and coolest. After activating the temperature gradient heater at Time = 0 to set a 0.03 K gradient, the target gradient was reached in 400 s. The intermediate point remained stable and exactly between the other two, suggesting that the present design achieves a uniform gradient. We plan to sequentially replace holders for the remaining analyzers.

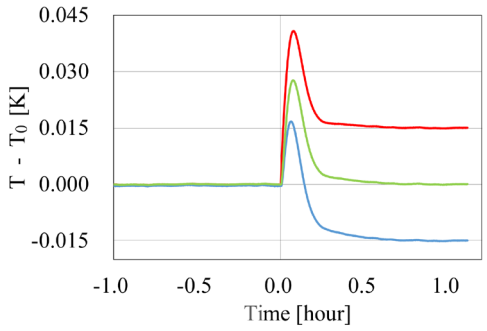

Fig. 4. Time variation of three temperatures (green: intermediate, red: high temperature part; cyan: low temperature part) on the same analyzer. The heater power was turned on at Time = 0. T_0 is the average intermediate temperature before Time = 0.

3. Nuclear resonant scattering

NRS activity on BL35XU provides a variety of techniques to investigate the electronic properties at specific nuclei, such as magnetism, valence state, and the local symmetry in specific atomic sites, and the dynamics in atomic or molecular systems. We have developed spectrometers and detectors tailored to each technique. We have a large number of high-resolution monochromators. This is because each isotope has a specific excitation energy, and the excitation energies of the targets vary from a few keV to ~90 keV, and each technique requires a different energy resolution, even if the techniques are applied to the same isotopes and excitation. The NRS activity uses not only conventional monochromators, which reflect monochromatic X-rays by Bragg diffraction, but also nuclear Bragg diffraction [5], which generates ultrahigh-resolution γ-rays with a ~neV–sub-μeV range at a specific single crystal with an appropriate magnetic structure of the isotope. Bunch-independent NRS techniques are available with these nuclear Bragg monochromators (NBMs). We have developed this type of NBM and a spectrometer-related synchrotron Mössbauer source [6] (SMS) providing γ-rays by nuclear Bragg diffraction.

SMS at the synchrotron radiation facility is mostly realized by using antiferromagnetic single crystals such as $FeBO_3$ and α-Fe_2O_3 to suppress the

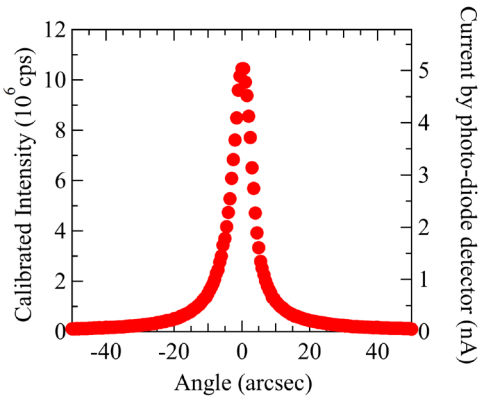

Fig. 5. Rocking curve of α-$^{57}Fe_2O_3$ 111 reflection.

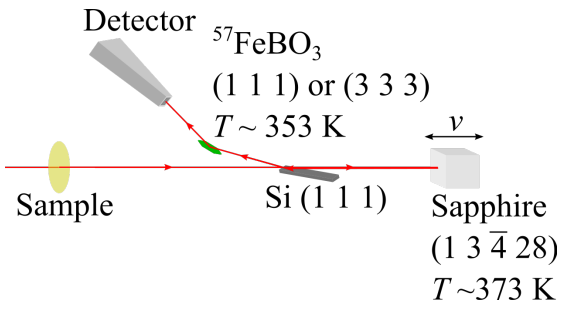

Fig. 6. Optics scheme for part of our SMS, downstream of the sample. The sapphire crystal oscillated by the Mössbaeur velocity driver makes the energy shift. Si (1 1 1) works to make a space afterward. The $^{57}FeBO_3$ crystal generates the γ-ray.

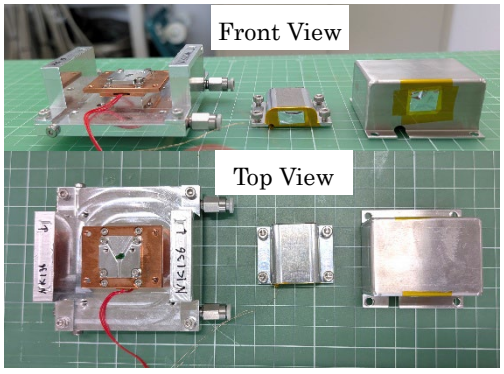

Fig. 7. Single crystal $^{57}FeBO_3$ in the furnace. $^{57}FeBO_3$ is mounted between two magnets (left). Two covers (middle and right) maintain the temperature, avoiding thermal radiation.

electronic scattering. Single crystal perfection is critical to obtain a high SMS flux, which contributes to good data quality. α-$^{57}Fe_2O_3$ single crystals grown by Dr. H. Takei [7] were evaluated by measuring the reflectivity from the 666 electronic reflection to obtain the best area and azimuthal angle of the crystals. By setting the best α-$^{57}Fe_2O_3$ crystal under the best condition, the SMS flux as high as 10 million counts/s, approximately double the previous value, has been obtained with the 111 pure nuclear reflection, as shown in Fig. 5.

SMS spectroscopy utilizing the $^{57}FeBO_3$ single crystal as the NBM is a powerful technique to enable ^{57}Fe energy domain hyperfine spectroscopy. The SMS spectroscopy is available now at BL11XU [8] and ESRF [9]. We are developing the SMS technique with an optical geometry different from the setups at these two facilities, as shown in Fig. 6. The sapphire and $FeBO_3$ crystals should maintain high temperatures, ~373 K and ~353 K, respectively. We designed the furnaces for them, and we have found that the furnaces have temperature stabilities within < 2mK rms, which is enough to obtain the SMS signal we want. The NBM crystal on the furnace is shown in Fig. 7.

FUKUI Hiroshi, MANJO Taishun, NAGASAWA Nobumoto, YODA Yoshitaka, and BARON Alfred
Precision Spectroscopy Division, JASRI

References:

[1] Ishikawa, D. & Baron, A. Q. R. (2010). *J. Synchrotron Radiat.* **17**, 12.

[2] Ishikawa, D. et al. (2015). *J. Synchrotron Radiat.* **22,** 3.

[3] Houtari, S. et al. (2005). *J. Synchrotron Radiat.* **12**, 467–472.

[4] Manjo, T. & Baron, A. Q. R. (2025) *J. Phys.: Conf. Ser.* **3010**, 012125.

[5] Smirnov, G. V. et al. (1969). *Pis'ma Zh. Eksp. Teor. Fiz.* **9**,123 [*JETP Lett.* (1970). **9**, 70].

[6] Smirnov, G. V. et al. (1997). *Phys. Rev. B* **55**, 5811.

[7] Suzuki, C. K. et al. (1993). *Jpn. J. Appl. Phys.* **32**, 3900.

[8] Mitsui, T, et al. (2009). *J. Synchrotron Radiat.*

16, 723.

[9] Potapkin, V. et al. (2012). *J. Synchrotron Radiat.* **19**, 559.